Contents lists available at Science-Gate

International Journal of Advanced and Applied Sciences

Journal homepage: http://www.science-gate.com/IJAAS.html

# Design of an MPPT charge controller using a DC–DC buck-boost converter under system disturbances

Abdulaziz J. Alateeq *

*Department of Electrical Engineering, College of Engineering, University of Ha'il, Ha'il, Saudi Arabia*

ARTICLE INFO

*Article history:*
Received 3 May 2025
Received in revised form
28 September 2025
Accepted 14 November 2025

*Keywords:*
Maximum power point tracking
Photovoltaic system
Buck-boost converter
Perturb and observe
PI controller

ABSTRACT

This paper presents the analysis and design of a maximum power point tracker (MPPT) for a 6 KW photovoltaic (PV) system. The MPPT is implemented through a DC–DC buck-boost converter, modeled and simulated in MATLAB/Simulink. The design begins with determining the operating point of the system by establishing the relationship between the converter's input impedance, output impedance, and duty ratio, which defines the mechanism of maximum power tracking under system disturbances such as variations in solar irradiance. To achieve optimal performance, the perturb and observe (P&O) algorithm is applied to track the maximum power point, generating a DC signal that is processed by a proportional–integral (PI) controller. The PI controller is designed using a mathematical model developed with the state-space approach, ensuring that the operating point of the system is maintained at the maximum power level.



## 1. Introduction

Renewable energy systems consist of various devices, which are designed to capture, manage, regulate, and store energy from renewable sources and supply it to the load. The charge controller is considered one of those devices, which is a power electronic circuit placed between the photovoltaic (PV) panels and the batteries. It performs as a DC-DC converter that regulates the system's voltage and current by adjusting its duty ratio to maximize the power generated by the PV panels and transfers it efficiently to the load. Also, the charge controller helps to extend the battery lifespan by preventing overcharging and deep discharging (Hamidi et al., 2020). There are two types of charge controllers, which are pulse width modulation (PWM) and maximum power point tracker (MPPT). The MPPT surpasses the PWM due to its ability to address a key challenge in renewable energy systems, which is the issue of providing less power to the load than the total potential power that can be generated by the photovoltaic (PV) array. MPPT can track the system operating point and regulate its voltage and current levels according to the load specifications by adjusting the converter's duty cycle and setting the operating point to its maximum.

Developing a functional DC-DC converter was impossible before the invention of semiconductor devices such as the bipolar junction transistor (BJT) in the 1950s and 1960s. These semiconductors functioned as switches, connecting and disconnecting the source from the load via a switching network. This sequence of connection and disconnection will generate a pulse signal to the load, which has to be filtered through a filter network to generate a DC signal that meets the load's specifications. DC-DC converters are generally categorized based on their power ratings into high-power and low-power applications. Renewable energy systems usually use high-power converters, which can be further classified into isolated and non-isolated converters. Isolated converters include topologies like flyback, push-pull, and half-bridge, while non-isolated converters include buck, boost, and buck-boost configurations. Other low-power applications, such as switched capacitor converters, are often utilized in integrated circuits (Guerra et al., 2021). The non-isolated high-power converters used in this project can be utilized for MPPT based on the input and output impedance values of the converter. When $R_{in}$ is larger than $R_O$, a buck converter can be used as an MPPT. Conversely, if $R_O$ is larger than $R_{in}$, a boost converter can be employed as an MPPT. However, a buck-boost converter can be utilized as an MPPT and is able to transfer maximum power from the source to the load, regardless of the values

* Corresponding Author.
Email Address: aj.alateeq@uoh.edu.sa
https://doi.org/10.21833/ijaas.2025.12.007
Corresponding author's ORCID profile:
https://orcid.org/0009-0008-3639-1687

of the converter's input and output impedances (Obeidi et al., 2022).

The DC-DC converter used in this work to design MPPT is a buck-boost converter, which has the ability to either step up or step down the input voltage. From Eq. 1, it is clear that if the duty ratio is more than 0.5, the converter performs as a boost. On the other hand, if the duty ratio is less than 0.5, it performs as a buck (Garcia and Strandberg, 2021).

The steady-state output voltage equation for a buck-boost converter is as follows:

$$V_o = V_s \frac{D}{1-D} \quad (1)$$

where, $V_o$ and $V_s$ are the converter's output voltage and input voltage, respectively. $D$ is the steady state Duty Cycle.

This converter is designed to handle and transfer 6.29 KW of DC power, which is harvested from 30 PV modules with $V_m = 29.6\,V$, $I_m =$ 7.09A, $V_{OC} =$ 35.9 $and$ $I_{SC} = 7.6$ A for each module and delivered to the load of $R = 2\ \Omega$. The array consists of 10 strings with 3 modules connected in series at each string (Ganesan and Gunasekaran, 2022).

The design of MPPT starts with the converter's sizing parameters. Then, introduce an open-loop uncontrolled MPPT to the system to explain how its operating point is determined and how the power transfers from PV arrays to the load. After that comes the necessity of designing a closed-loop controlled MPPT in case of a disturbance introduced to the system (Maidin et al., 2020).

If a disturbance is introduced to the system shown in Fig. 1, an algorithm is required to track and return the system's operating point to its maximum. The algorithm used in this project is Perturb and Observe (Salman et al., 2018), which is widely utilized in MPPT applications (Restrepo et al., 2021). It is recognized for its simplicity and reasonable accuracy. However, it is not ideal for applications with quick changes in irradiance due to the oscillation it causes around the maximum power point. Other algorithm techniques, such as short circuit current (SCC) (Byanpambé et al., 2024), constant voltage algorithm (CV) (Celikel et al., 2022), and incremental conductance (IC) (Shang et al., 2020) methods, are widely integrated in MPPT applications. Each of them has its own advantages and disadvantages in terms of accuracy, speed, and complexity. For instance, the IC method is considered to be more complex than P&O; it responds faster than P&O and provides greater accuracy at the MPP.

However, it is more sensitive to noise and demands higher computational resources. The CV algorithm is suitable for applications with stable conditions. It is considered to be the poorest among other algorithms in terms of complexity and accuracy. Yet, it delivers a fast response despite its simplicity and low implementation cost.

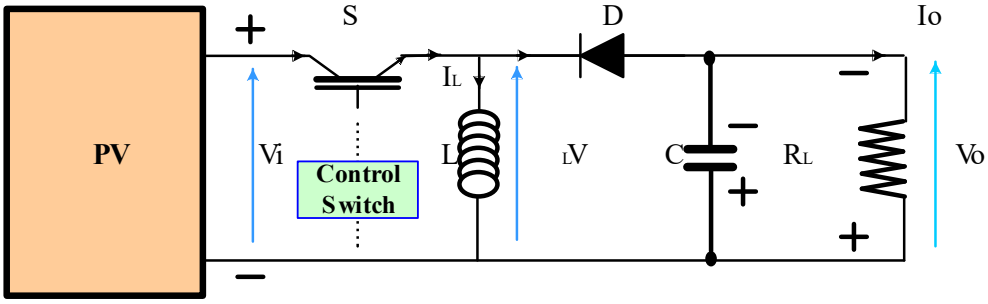


**Fig. 1:** DC-DC buck boost converter used as MPPT

In recent years, a set of MPPT techniques has been proposed for PV applications. Among these, several techniques are based on classical methods such as P&O, IC, and SCC. For instance, Anbuchandran et al. (2024) have combined P&O with an improved version of the invasive weed optimization (IWO) algorithm to find the GMPP. In the proposed method, the IWO algorithm is used to find the optimal MPP; then, P&O is applied to adjust the optimal solution by modifying the operating conditions and observing the output changes. Another technique combining P&O and the particle swarm optimization (PSO) algorithm was developed by Ibrahim et al. (2023) for extracting the maximum power from a PV module. The decision variables in the PSO algorithm were the voltage and current of the PV panel, while the objective function was the generated power of the full system. The obtained values of the PV voltage and current were adopted to adjust the step size of the P&O method. To address limitations of the IC method, Anowar and Roy (2019) suggested a PI regulator to eliminate the error between the incremental (dI/dV) and the actual (I/V) conductance. The PI regulator output was considered as the converter duty cycle. Alongside these techniques, various intelligent approaches have emerged in the MPPT algorithms, such as artificial neural networks (Gul et al., 2024), fuzzy logic (Melhaoui et al., 2025), and machine learning (Hamad et al., 2025). Furthermore, other hybrid strategies combining conventional methods and intelligent techniques, such as genetic algorithms and P&O (Salman et al., 2018), have been developed in the literature to determine GMPP. Although this approach offers a superior control process compared to other algorithmic methods, it has drawbacks, including weak real-time performance, high complexity, and limited practicality (Masry et al., 2023). Despite the diversity of MPPT techniques, it remains difficult to definitively decide which one is

the most robust and effective. However, according to a bibliographic study, it has been found that a wide range of MPPT techniques are based on P&O methods due to their simplicity and reasonable accuracy (Endiz et al., 2025).

The main idea of the P&O algorithm is to periodically vary the operating voltage of the PV module or the duty cycle of the converter. If the PV power increases, the algorithm keeps the disturbance of the voltage in the same direction (increase or decrease). However, if it decreases, the algorithm disturbs the voltage in the opposite direction (Salman et al., 2018). Within this context, a P&O-based MPPT controller combined with a buck-boost converter is presented and implemented in this study. Unlike several converters, the DC-DC converter is designed to track the MPP under a wide range of load resistances. To do this, a methodology for sizing and adjusting the buck-boost converter parameters is developed. Analysis of the dynamic response of the suggested MPPT controller, through simulation tests and comparison with other methods, showed its effectiveness under various load conditions.

## 2. Converter operation principle

To understand the MPPT mechanism or operation principle of transferring maximum power to the load, first, we need to understand how the power flows from a single PV module to the load directly without MPPT (Ríos et al., 2020). Since PV is a current source, the maximum power delivered to a load is limited to a single value of the load as in Eq. 2.

$$R_m = \frac{V_m}{I_m} \quad (2)$$

where, $V_m$ and $I_m$ are the PV's maximum voltage and maximum current, respectively. $R_m$ is the maximum impedance.

This relationship indicates that maximum power can only be delivered when the PV system, with these specifications, is connected to $R_m$. If the load changes for any reason, the system will no longer be able to deliver maximum power. Additionally, if a disturbance affects the system and alters the PV specifications, a new value of $R_m$ must be connected to the PV to ensure its capability of delivering maximum power.

This principle can be illustrated by using the module with specifications mentioned earlier. Under standard test conditions (STC), the module is able to generate a current of $I_m = 7.09\ A$ and $V_m = 29.6\ V$ with maximum power of $P_m = 209.8\ W$. Using Eq. 2, this module will generate maximum power only if it is connected to a load of size.

$$R_m = \frac{V_m}{I_m} = \frac{29.6}{7.09} = 4.17\ \Omega$$

Any other values for the load will drift the system's operating point away from its maximum power point. For example, if 2 Ω is used instead of 4.17Ω, the module will generate a current close to $I_{SC}$ which is approximately $I = 7.4\ A$ under STC, as shown in Fig. 2a. Since the PV is a current source which means that the current is fixed and the voltage developed across the load depends on its size, a voltage of $14.8\ V$ will be developed across it, as in Fig. 2b. The power this module is able to deliver under STC is only $109.5\ W$, Fig. 2c. Whereas this module has the potential to generate $209.8\ W$ with the appropriate value of $R$.

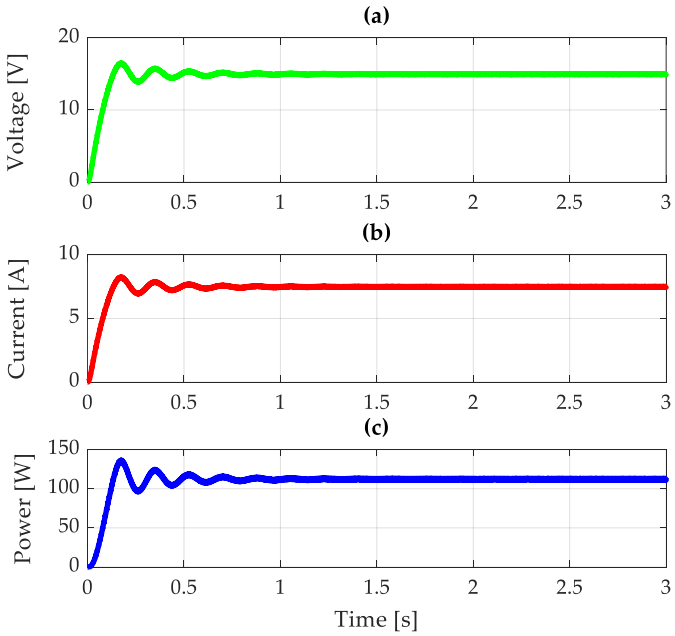


**Fig. 2:** System response without MPPT: (a) voltage, (b) current, (c) power

For this reason, a power electronics DC-DC converter, such as a Buck-Boost, is needed in renewable energy systems to transfer the maximum power to the load. This DC-DC converter is able to

track the maximum power and deliver it by adjusting its control input, which is a time-varying variable known as the duty ratio $d$ (Tirado-Serrato et al., 2024). As the load changes, the converter's duty ratio has to be changed accordingly through a control process to set the system operating point back to its maximum (Table 1). However, those changes that occur to the load do not influence the output voltage Eq. 1, which means that the appropriate value of duty ratio cannot be calculated for this equation. Therefore, another equation that presents the relationship between the converter's input and output impedances is needed. So, if any changes occur to the load or the PV's specification, a new duty ratio can be calculated and provided to the converter's switch to track the maximum power. This equation is as follows:

$$D = \frac{1}{1+\sqrt{\frac{R_t}{R_o}}} \quad (3)$$

where, $R_t$ and $R_o$ are the converter's input impedance and converter's output impedance, respectively.

Using the same example mentioned earlier with $R_O = 2\Omega$ connected to the PV module without MPPT, the power delivered to the load is around 110 W, as in Fig. 2. However, the maximum power of 209.8 $W$ is going to be delivered to the load by adjusting the appropriate value of $d$. This MPPT is going to sense the PV module's voltage ($V_m = 29.6\,V$) and current ($I_m = 7.09\,A$), then calculate the converter's input impedance $R_t = 4.17\,\Omega$.

**Table 1:** Values of $d$ to deliver maximum power to a variety of loads

| Load resistance (Ω) | Duty ratio |
|---|---|
| 2 | 0.409 |
| 5 | 0.522 |
| 10 | 0.607 |
| 15 | 0.655 |
| 20 | 0.686 |
| 30 | 0.728 |
| 40 | 0.756 |
| 50 | 0.776 |

Using Eq. 3, the new duty ratio equals 0.409, which can be substituted back in Eq. 1 to find the converter output voltage $V_o = 20.48\ V$, this means that the converter is acting as a buck. So, as in Fig. 3, the power delivered to the load can be calculated as follows.

$$P_m = \frac{V_o^2}{R_o} = \frac{20.48^2}{2} = 209.7\ W.$$

In practical life, parameters of renewable energy systems are constantly changing. The disturbance occurs in the system, which can be a variation in the irradiance isolation, which has a direct effect on the PV current. This adjustment will make changes to the converter's input impedance $R_t$. So, a new duty ratio for the buck-boost converter is required to deliver the maximum power.

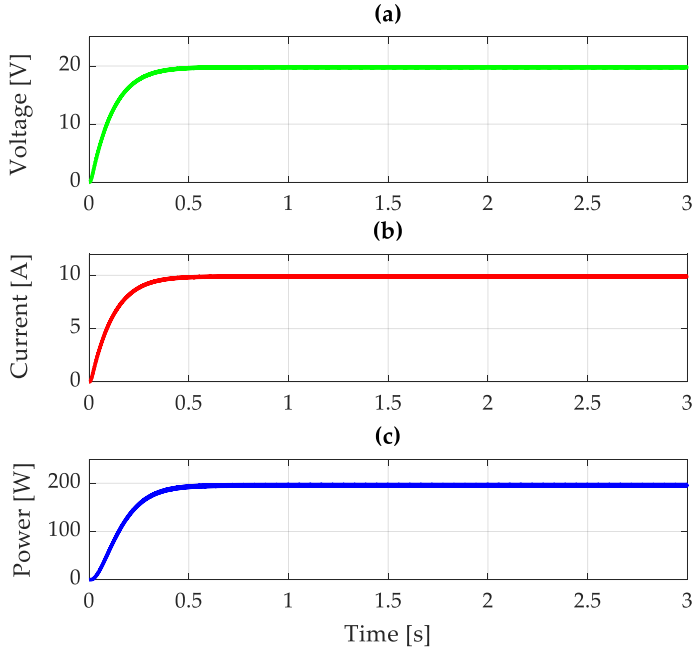


**Fig. 3:** System response with MPPT: (a) voltage, (b) current, (c) power

## 3. Perturb and observation algorithm

The algorithm used in this project to track the maximum power point is perturb and observe. The operating principle of this algorithm is based on a constant comparison between voltage and power supplied by the PV array to identify the system operating point and take the appropriate action. Since the system's voltage and power are continuously fluctuating due to environmental conditions, it is a crucial part of the algorithm process to determine whether the system's voltage and power are increasing or decreasing (Yilmaz, 2024). This task can be achieved by comparing the system's present and past operating points for both voltage and power. The system's past operating

point can be determined by applying a delay to the system's present point. If the previous operating point is subtracted from the present one and the result is positive, it indicates that the signal of the voltage or the power is increasing. Conversely, if the result is negative, it means the signal is decreasing (Gil-Velasco and Aguilar-Castillo, 2021). The flowchart in Fig. 4 illustrates the conditions for incrementally increasing or decreasing the voltage based on the comparison between the system voltage and power. The system voltage has to be increased if the maximum power point is forward, which occurs when the system's voltage and power both are increasing, or both are decreasing. On the other hand, the system voltage has to be decreased if the maximum power point is reversed, which occurs when the system's voltage and power are increasing or decreasing in opposite directions of each other.

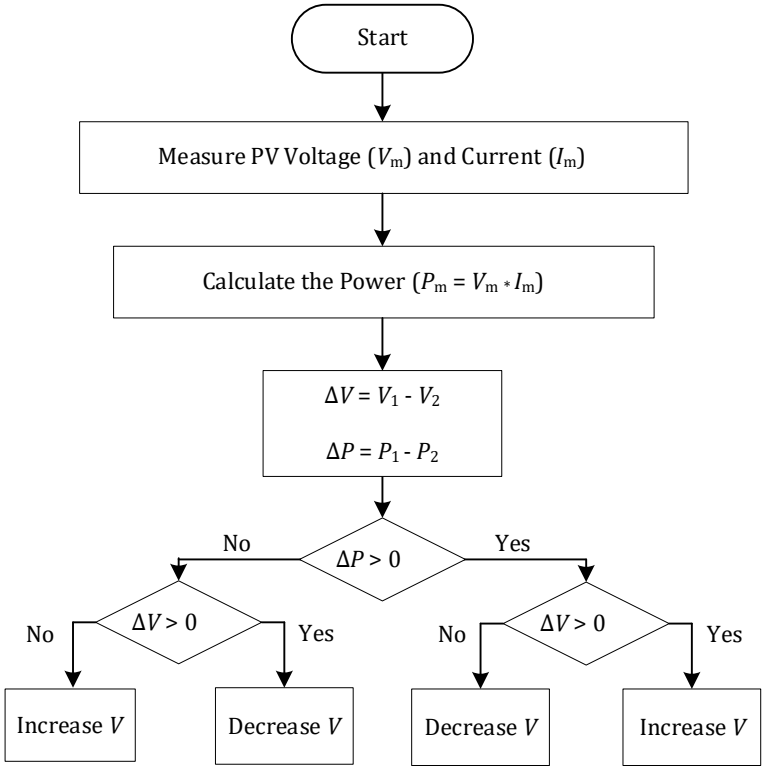


**Fig. 4:** Flow chart for perturb and observe algorithm

The utilization of the perturb and observe algorithm in MATLAB Simulink is presented in Fig. 5. It starts by sensing the present signals for the system's voltage and current, which are then multiplied together to calculate the system's power signal. A sample of those signals passes through a delay to generate the previous version of the system's voltage and power signals. Then, the present and past signals are compared using a comparator to determine whether the system voltage is increasing or decreasing. The result of this comparison is sent to two switches (Ali et al., 2023). The first switch applies a positive increment to the positive input terminal and a negative increment to the negative input terminal. The second switch is connected in the opposite manner. The same process is then applied to the power signal; the comparison outcome is sent to the switch with positive input terminal connected to the output of switch 1 and its negative input terminal connected to the output of switch 2. The generated signal will pass through a saturation block to restrict the increments to the maximum and minimum voltages, which are determined by the highest and lowest voltages that the PV array can produce. This process is continuously repeated until the incremented voltage signal matches the reference signal (Mahmod Mohammad et al., 2020).

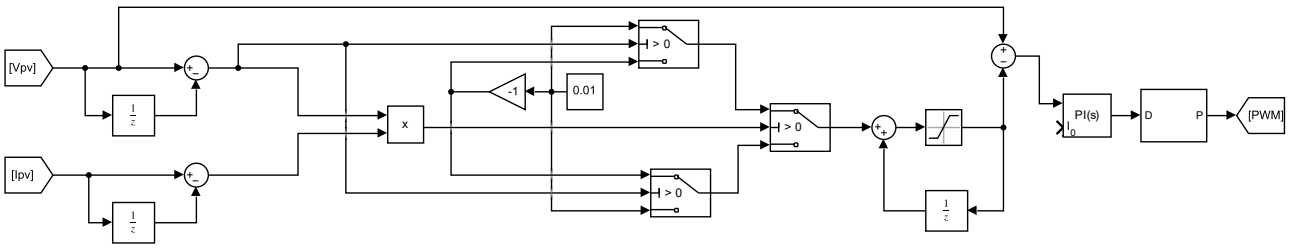


**Fig. 5:** Perturb and observe algorithm in MATLAB Simulink

Although the P&O algorithm offers several advantages for renewable energy systems, it also has limitations that can affect performance under certain conditions. First, the algorithm often causes

oscillations around the maximum power point (MPP) because it continuously compares and adjusts the operating point, preventing full stabilization. Second, the algorithm has a relatively slow tracking speed, which may reduce its ability to follow the MPP accurately. However, changes in solar irradiance and ambient temperature usually occur gradually, giving the algorithm enough time to respond; therefore, this drawback mainly appears during rapid environmental changes. A third limitation is the algorithm's tendency to converge to a nearby local maximum rather than the true global MPP, which can reduce the overall power output.

## 4. Converter sizing parameter

The buck-boost DC-DC converter consists of a switching network that performs as a single-pole double-throw switch and a filter network to filter the pulse signal generated by the switch Fig. 1. The converter input terminal has to withstand the maximum PV array output voltage for the cases with or without load (Cubas et al., 2017). Under standard test conditions, in the case of no load, PV output voltage can generate 108 V, which is three times the open circuit voltage $V_{OC}$, whereas, in the case of with load, the PV array will generate a total of 89 V and 70.9 A. Less voltage at the converter input terminal can be measured in the case of with-load; yet, a large amount of current is going to flow through the converter components, such as switching and filter networks, which need to be carefully designed to withstand the amount of power supplied to the system.

Sizing the converter's inductors can be determined by the following equation:

$$L_{min} = \frac{(1-D)^2 R}{2f} \quad (4)$$

where, $f$ is the switching frequency, which is 10 KHz.

Since the duty ratio $D$ varies from 0 to 1, the inductor size also varies because it is a function of the duty ratio, as in Eq. 4. So, $L$ has to be sized carefully to make sure the current is in continuous mode. For this reason, the minimum value for the inductor has to be the maximum value that can be acquired from Eq. 4, which in this case $D$ is zero.

Sizing the converter's capacitor can be determined from the following equations:

$$C = \frac{D}{Rf\frac{\Delta V_O}{V_O}} \quad (5)$$

where, $\Delta V_O$ is the output voltage ripple.

## 5. Converter control design

The previous analysis of the buck-boost DC-DC converter was based on an open-loop, uncontrolled system, which is not applicable for renewable energy applications (Deraz et al., 2024). To enable control of this converter, a mathematical model is required to design a closed-loop controlled DC-DC converter.

In the case of a buck-boost converter, a dynamic model for this converter can be developed by a set of differential equations represented in state-space form.

$$\dot{x} = Ax + Bu$$
$$y = Cx + Du$$

To develop a state-space model for this converter, first identify the energy storing elements, which are the capacitor and inductor. Second, identify the variables that will be used for modeling, which are the input variables, noted as $u$ and the state variable noted as $x$. The system input vector is the input voltage $v_{in}$, and duty ratio $d$. Also, the system state vector is the capacitor voltage $v_C$ and inductor current $i_L$. The state space model for the buck-boost converter can be written using those variable vectors plus the converter parameters, which are $R, C, and\ L$. The system order is determined by the number of dynamic elements, which is represented by differential equations. Third, segregate those differential equations into the following form

$$\dot{x} = Ax + Bu$$
$$y = Cx + Du$$

From this state-space model, a single-input single-output transfer function can be developed for the buck-boost converter. This transfer function describes the dynamic relationship between the control output $V_O$ and the control input $d$.

The control process is utilized by sensing the control output signal and converting it into a low-power information signal. This signal is then fed back to the comparator, where it is compared to the reference output signal to generate an error signal. The goal of the controller is to adjust the control input $d$ so that the error signal is minimized to zero (Zambrano-Gutierrez et al., 2022).

The switching network in the buck-boost converter consists of an uncontrolled switch diode, and a controlled switch IGBT, which is governed by the pulse signal control input $d$. This means that the converter has two different topologies; the first topology is formed during a fraction of the time $dT$ when the switch is ON, whereas the second topology is formed during the rest period of time, which is $(1-d)T$ when the switch is OFF. To develop a state-space model for this converter with two different topologies, a circuit averaging method is needed to combine the two different topologies and bring them together into one single averaged state-space large signal model (Khan et al., 2024).

The state space model for the converter's first topology (Fig. 6), during the period of $dT$ is as follows:

$$\begin{bmatrix} \dot{i_L} \\ \dot{v_C} \end{bmatrix} = \begin{bmatrix} 0 & 0 \\ 0 & -\frac{1}{RC} \end{bmatrix} * \begin{bmatrix} i_L \\ v_C \end{bmatrix} + \begin{bmatrix} \frac{1}{L} \\ 0 \end{bmatrix} * [v_{in}]$$

$$[y] = [0 \quad 1] * \begin{bmatrix} i_L \\ v_C \end{bmatrix} + [0] * [v_{in}]$$

The state space model for the converter's second topology (Fig. 7), during the period of $(1-d)T$ is as follows:

$$\begin{bmatrix} \dot{i_L} \\ \dot{v_C} \end{bmatrix} = \begin{bmatrix} 0 & -\frac{1}{L} \\ \frac{1}{C} & -\frac{1}{RC} \end{bmatrix} * \begin{bmatrix} i_L \\ v_C \end{bmatrix} + \begin{bmatrix} 0 \\ 0 \end{bmatrix} * [v_{in}]$$

$$[y] = [0 \quad 1] * \begin{bmatrix} i_L \\ v_C \end{bmatrix} + [0] * [v_{in}]$$

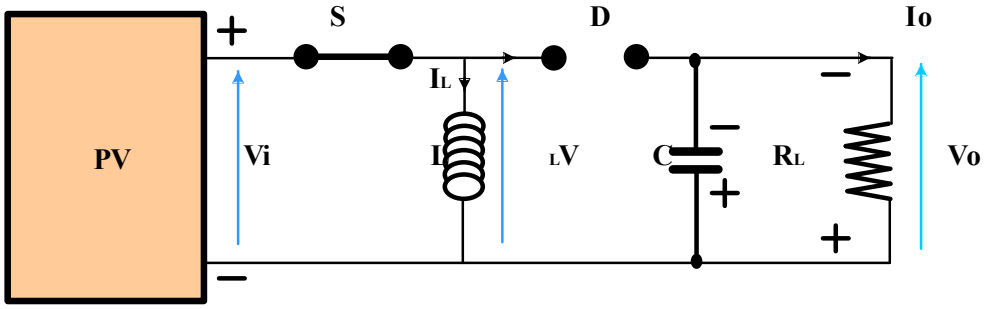


**Fig. 6:** Buck-boost converter topology with switch ON

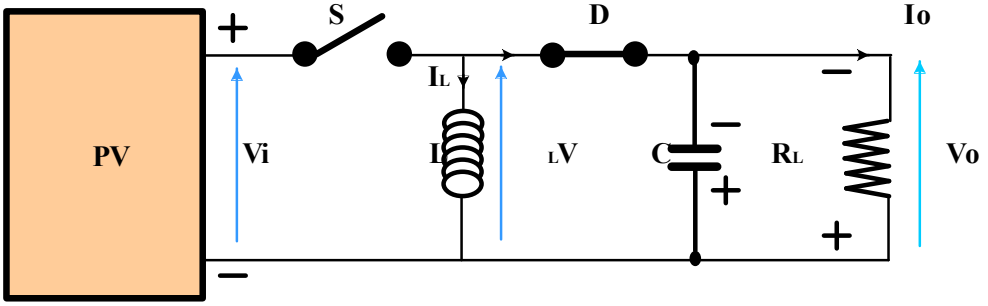


**Fig. 7:** Buck-boost converter topology with switch OFF

The two-state space model of the buck boost converter can be combined based on the following averaging method

$$A = A_1 * d + A_2 * (1-d)$$
$$B = B_1 * d + B_2 * (1-d)$$
$$C = C_1 * d + C_2 * (1-d)$$
$$D = D_1 * d + D_2 * (1-d)$$

where, the state space matrix $A$ represent the weighted average $A_1$ matrix during the period of $dT$ plus the weighted average $A_2$ matrix during the period $(1-d)T$. The same method can be applied to the rest of the state space matrices $B, C$ and $D$. After combining the two state space models for this system, an averaged large signal state space model is as follows:

$$\begin{bmatrix} \dot{i_L} \\ \dot{v_C} \end{bmatrix} = \begin{bmatrix} 0 & -\frac{1-d}{L} \\ \frac{1-d}{C} & -\frac{1}{RC} \end{bmatrix} * \begin{bmatrix} i_L \\ v_C \end{bmatrix} + \begin{bmatrix} \frac{d}{L} \\ 0 \end{bmatrix} * [v_{in}]$$

$$[y] = [0 \quad 1] * \begin{bmatrix} i_L \\ v_C \end{bmatrix} + [0] * [v_{in}]$$

This averaged large signal model for the buck-boost converter becomes a time-varying model, which means that it is a nonlinear state-space model. So, it cannot be used directly for controller design applications. For this reason, the linearization process is required to make this model applicable for control applications (Koundi et al., 2022).

Since the input variables and the state variables in the large signal model consist of a steady-state part and a small signal part, the linearization process is utilized by removing the steady-state part from the large signal model, which makes it a time-invariant model (Al-Baidhani et al., 2023).

$$(\dot{X + \hat{x}}) = A(X + \hat{x}) + B(U + \hat{u})$$
$$(\dot{X + \hat{x}}) = [A_1 * (D + \hat{d}) + A_2 * (1 - (D + \hat{d}))](X + \hat{x}) + [B_1 * (D + \hat{d}) + B_2 * (1 - (D + \hat{d}))](U + \hat{u})$$

Some simplifications can be applied to the large signal model by setting the steady-state terms directly to zero. Meanwhile, for the remaining terms, which have the product of two small signals, they become very small terms that can be neglected. After the simplification process and removing the steady state part, the system's small signal model can be written as follows:

$$\dot{x} = A\hat{x} + B\hat{u} + [(A_1 - A_2)X + (B_1 - B_2)U]\,\hat{d}$$

The state matrices $A$ and $B$ are steady state matrices, which means that the time varying variable $d$ is changed to the steady state variable $D$ as follows

$$A = \begin{bmatrix} 0 & -\frac{1-D}{L} \\ \frac{1-D}{C} & -\frac{1}{RC} \end{bmatrix}$$

$$B = \begin{bmatrix} \frac{D}{L} \\ 0 \end{bmatrix}$$

$$A_1 - A_2 = \begin{bmatrix} 0 & 0 \\ 0 & -\frac{1}{RC} \end{bmatrix} - \begin{bmatrix} 0 & -\frac{1}{L} \\ \frac{1}{C} & -\frac{1}{RC} \end{bmatrix} = \begin{bmatrix} 0 & \frac{1}{L} \\ -\frac{1}{C} & 0 \end{bmatrix}$$

$$B_1 - B_2 = \begin{bmatrix} \frac{1}{L} \\ 0 \end{bmatrix} - \begin{bmatrix} 0 \\ 0 \end{bmatrix} = \begin{bmatrix} \frac{1}{L} \\ 0 \end{bmatrix}$$

The linearized small signal state-space model for the buck boost converter can be written as follows:

$$\begin{bmatrix} \dot{\iota_L} \\ \dot{v_C} \end{bmatrix} = \begin{bmatrix} 0 & -\frac{1-D}{L} \\ \frac{1-D}{C} & -\frac{1}{RC} \end{bmatrix} * \begin{bmatrix} \widehat{\iota_L} \\ \widehat{v_C} \end{bmatrix} + \begin{bmatrix} \frac{D}{L} \\ 0 \end{bmatrix} * [\widehat{v_{in}}] + \left( \begin{bmatrix} 0 & \frac{1}{L} \\ -\frac{1}{C} & 0 \end{bmatrix} * \begin{bmatrix} I_L \\ V_C \end{bmatrix} + \begin{bmatrix} \frac{1}{L} \\ 0 \end{bmatrix} * [V_{in}] \right) * [\hat{d}]$$

$$\begin{bmatrix} \dot{\iota_L} \\ \dot{v_C} \end{bmatrix} = \begin{bmatrix} 0 & -\frac{1-D}{L} \\ \frac{1-D}{C} & -\frac{1}{RC} \end{bmatrix} * \begin{bmatrix} \widehat{\iota_L} \\ \widehat{v_C} \end{bmatrix} + \begin{bmatrix} \frac{D}{L} \\ 0 \end{bmatrix} * [\widehat{v_{in}}] + \begin{bmatrix} \frac{V_{C+}V_{in}}{L} \\ -\frac{I_L}{C} \end{bmatrix} * [\hat{d}]$$

Since the control input has been chosen to be the small signal duty ratio $\hat{d}$ and the control output is the output voltage $V_O$, the state space input voltage can be deleted.

$$\begin{bmatrix} \dot{\iota_L} \\ \dot{v_C} \end{bmatrix} = \begin{bmatrix} 0 & -\frac{1-D}{L} \\ \frac{1-D}{C} & -\frac{1}{RC} \end{bmatrix} * \begin{bmatrix} \widehat{\iota_L} \\ \widehat{v_C} \end{bmatrix} + \begin{bmatrix} \frac{V_{C+}V_{in}}{L} \\ -\frac{I_L}{C} \end{bmatrix} * [\hat{d}]$$

After calculating all the converter parameters, the converter state space small signal models are as follows:

$$\begin{bmatrix} \dot{\iota_L} \\ \dot{v_C} \end{bmatrix} = \begin{bmatrix} 0 & -44.2 \\ 884 & -1000 \end{bmatrix} * \begin{bmatrix} \widehat{\iota_L} \\ \widehat{v_C} \end{bmatrix} + \begin{bmatrix} 20135 \\ -254202 \end{bmatrix} * [\hat{d}]$$

The system transfer function can be computed from the developed small signal model by MATLAB software. This transfer function $G_S$ describes the relationship between the control input small signal $\hat{d}$ and the control output voltage $V_O$, which is needed to design the controller.

$$[y] = [0 \quad 1] * \begin{bmatrix} \dot{\iota_L} \\ v_C \end{bmatrix} + [0] * [\hat{d}]$$

Computing the converter parameters is necessary to develop the state-space small signal model for the buck-boost converter, as shown in Fig. 8 (Tomaszuk and Borawski, 2024). The first parameter that has to be calculated is the duty ratio, which is presented in Eq. 3. The load connected to the converter is $R_O = 2\Omega$, while the converter's input impedance can be calculated using Ohm's law. Considering the PV array's maximum voltage $V_m = 89V$ and the array current $I_m = 71A$, the converter input impedance $R_O$ is determined to be 1.25 Ω. Thus, using the duty ratio relationship presented in Eq. 3, the resulting duty cycle $d$ is 0.558. Then, the converter inductor can be computed using Eq. 4, which sizes the minimum value of the inductor to stay in the current continuous mode (Xie et al., 2023). Since this equation is a function of the duty cycle $d$, it is possible that $d$ goes to zero, and the inductor is at its minimum value. So, by choosing $d$ equal zero, $L_{min}$ is calculated to be 100 $uH$. Yet, this value is the minimum size of the inductor to stay in CCM. However, for stability and optimal system response, the inductor value needs to be much larger than that and is chosen to be 20 $mH$. The last parameter is the capacitor, which can be sized using Eq. 5. Setting the output voltage ripple to be no more than 10% of the output voltage, it is computed to be around 300 $uf$. Again, for more stability and better system response, the capacitor is chosen to be 500 $uf$ (Hinov et al., 2023).

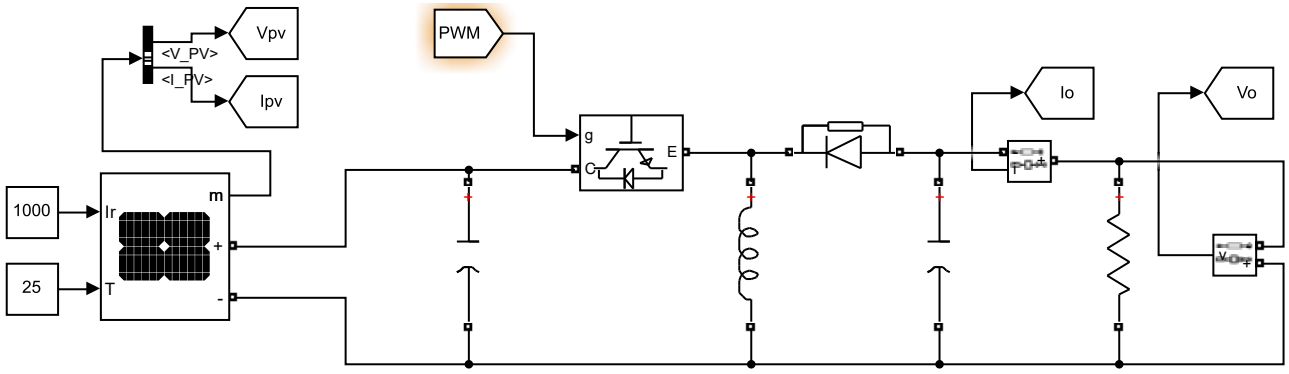


**Fig. 8:** DC-DC buck boost converter used as MPPT in MATLAB Simulink

$$G_S = \frac{-2.5 * 10^5 S + 1.7 * 10^7}{S^2 + 1000 S + 3.9 * 10^4}$$

The system transfer function is going to be convoluted with the control's transfer function $G_C$ which, consists of a proportional part and an integral part. The resulting transfer function is going to be convoluted again with the feedback loop transfer function $G_H$ to form the system's overall transfer function as follows

$$G_S = \frac{K\, G_S\, G_C}{1 + K\, G_S\, G_C\, G_H}$$

Since the system's transfer function has a zero in the right of the S-plane, the root locus method is going to be used to design a controller instead of the Bode plot approach.

From the root locus (Fig. 9), the control gain $K$ is picked and substituted into the system transfer function $G_S$ to get its step response. By keeping changing the control gain $K$, the best step response of the system is determined, and the controller design is completed.

After completing the control design and tuning the control parameter properly, MPPT is able to track the maximum power of 6.29 KW of DC power and deliver it to the load as presented in Fig. 10.

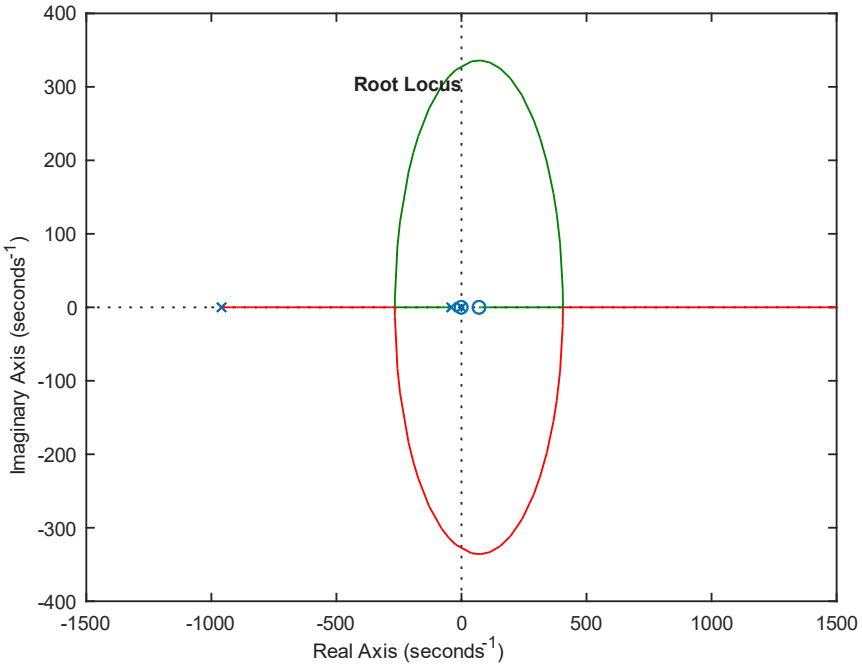


**Fig. 9:** Root locus for the system transfer function

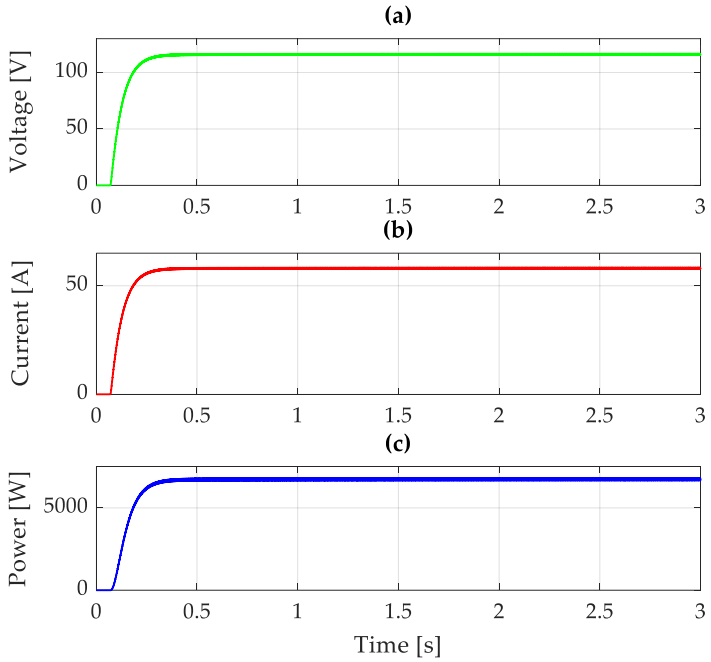


**Fig. 10:** System response of tracking the maximum power: (a) voltage, (b) current, (c) power

Results in Fig. 11 show the system response under STC with $R_O = 2\ \Omega$ and $R_O = 5\ \Omega$. The system is able to track the maximum power with different loads.

Fig. 12 shows the system response when the insolation dropped to 500 $W/m^2$, which is going to reduce the generated power to almost 3000 $W$.

Because the PV module parameters are sensitive to the ambient temperature, the system's voltage and current change as the ambient temperature varies. Those modifications to the system parameters will have a direct effect on the amount of power delivered to the load as the system's operating point shifts away from its maximum.

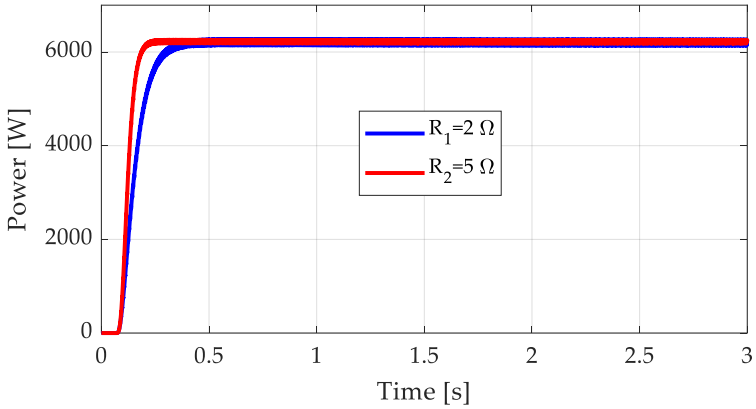


**Fig. 11:** System response of tracking the maximum power with $R_O = 2\Omega$ and $R_O = 5\Omega$

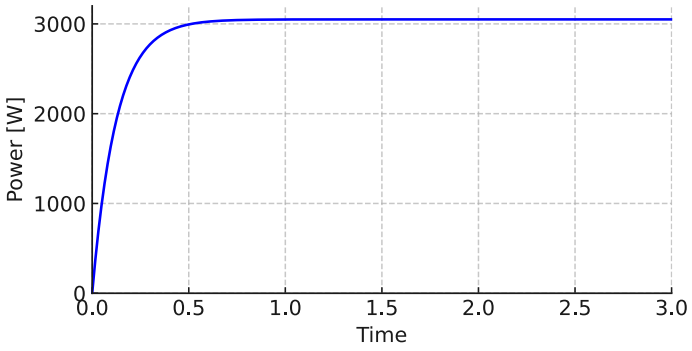


**Fig. 12:** System time response with insulation drooped to 500 $W/m^2$

The voltage temperature coefficient of the PV modules used in this project is -0.33%, indicating that the voltage decreases by 0.33% for every 1°C rise in temperature. Also, the current temperature coefficient is 0.057%, meaning the current increases by 0.057% per degree Celsius increase in temperature. To evaluate the impact of those temperature coefficients on MPPT performance, it is essential to measure the system's voltage and current under different ambient temperature conditions. For instance, when the ambient temperature reaches 50°C, the updated module voltage can be determined using the following method:

$$V_{new} = V_{mp} + \left[(Temp - STC) * \left(\frac{(V_{mp})\ Temp\ Coefficient}{100}\right) * V_{mp}\right] \quad (6)$$

$$V_{new} = 29.6 + \left[(50 - 25) * \left(\frac{-0\ 0.33}{100}\right) * 29.6\right]$$

$$V_{new} = 29.6 + (-2.44) = 27.16\ V$$

A similar approach can be applied to determine the module's new current at an ambient temperature of 50 °C, as outlined below:

$$I_{new} = I_{mp} + \left[(Temp - STC) * \left(\frac{(I_{mp})\ Temp\ Coefficient}{100}\right) * I_{mp}\right] \quad (7)$$

$$I_{new} = 7.09 + \left[(50 - 25) * \left(\frac{0.057}{100}\right) * 7.09\right]$$

$$I_{new} = 7.09 + 0.1 = 7.19\ A$$

The power that this module is able to generate at 50 °C is:

$$P_{new} = 27.16 * 7.09 = 192\ W$$

The new values of the module parameters can be applied to the photovoltaic (PV) array configuration used in this project. Since the system consists of 10 strings with 3 modules in each string, the system yields a new voltage of 81.48 V and a new current of 71.9 A. Thus, the system is capable of generating a maximum power output of approximately 5.86 kW, which represents a 6.83% drop in power generated under Standard Test Conditions (STC). The MPPT controller is able to deliver the maximum power to the load if the duty ratio is accurately adjusted to the appropriate value.

At an ambient temperature of 50°C, the revised MPPT duty cycle can be determined using Eq. 3, which involves calculating the system's input impedance, found to be $R_t = 1.13\ \Omega$.

$$D = \frac{1}{1 + \sqrt{\frac{R_t}{R_o}}} = \frac{1}{1 + \sqrt{\frac{1.13}{2}}} = 0.57$$

With a duty cycle of 0.57, the system is able to track the maximum power generated at an ambient temperature of 50°C as presented in Fig. 13.

Another extreme ambient temperature of 0°C is applied to the PV module that is used in this project to calculate the new output power. From Eqs. 6 and 7, the system's new values of voltage and current are calculated and found to be 32 V and 6.98 A, respectively. The amount of power this module is able to generate at a temperature of 0°C equals 223 W, which represents a 6% increase in the generated

power at STC. This means that a maximum power of 6.69 kW is able to be generated from the PV array used in the project at an ambient temperature of 0 °C. The system is operating at a voltage of 96 V and a current of 69.8 A, which results in a system input impedance of $R_t = 1.13\ \Omega$ and a duty cycle of 0.54. Fig. 13 presents the system response at ambient temperatures of 0°C and 50°C. It shows that the system is able to track the maximum power at different conditions with a stable response.

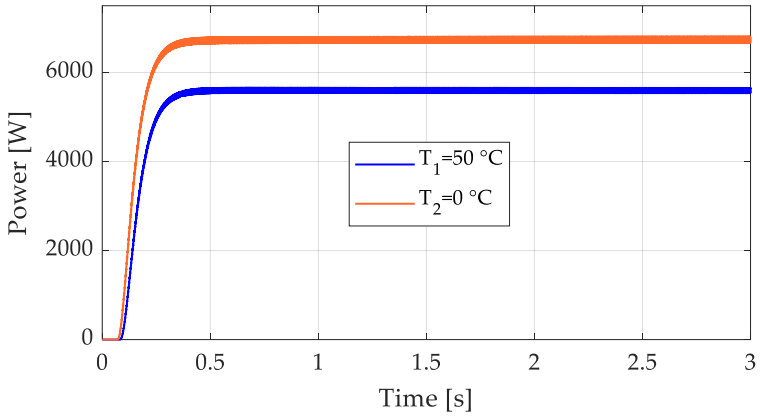


**Fig. 13:** System response of tracking the maximum power at temperatures of 0°C and 50°C

Table 2 presents a comparative analysis between the data obtained from the O&P algorithm used in this paper and the fuzzy logic control method presented in Abbas et al. (2025). The FLC method presents a faster response than P&O in tracking speed, settling time, and in response to rapid changes. Whereas, the P&O presents less implementation complexity than the FLC method.

**Table 2:** Comparative analysis between O&P and FLC methods

| Algorithm | Perturb and observe | Fuzzy logic control |
|---|---|---|
| Tracking speed | Moderate | Very Fast |
| Settling time (ms) | 0.4 | 0.006 |
| Implementation complexity | Low | High |
| Response to rapid changes | Low | Fast |
| Oscillation at MPPT | Moderate | Low |

## 6. Conclusions

In this paper, a complete design of an MPPT is introduced in simulation and mathematical modulation. The DC-DC converter used in this design is a buck-boost converter, which can track the maximum power point the value of the load $R$. Unlike other converters, which has a limited range of load values that the converter is able to track MPP with.

The main scope of this paper is to provide a comprehensive explanation of MPPT design and its response to disturbances in renewable energy applications. The design starts by determining the appropriate size of the inductor, which is a key part of MPPT design, in order to ensure a continuous flow of current. Since $L_{min}$ is a function of $d$, which is a time-varying variable ranging from 0 to 1, the minimum value of $L_{min}$ occurs when $d$ = 0, resulting in $L$ = 100µ. Any inductor smaller than this value will cause the system to exhibit an unstable response. Therefore, $L$ must be selected to be much larger than this value, specifically $L$ = 20mH.

Regarding capacitor sizing, it is determined by the ratio of the output voltage ripple to the output voltage, which has been set to approximately 10%.

The state-space small-signal model developed for the buck-boost converter includes several input and output parameters. The system's input parameters are the input voltage and duty ratio $d$, while the output parameters are the output voltage and output current. The goal of developing the small-signal model for the buck-boost converter is to derive a single-input, single-output (SISO) transfer function using MATLAB software. Since this transfer function will be used to design a controller for the converter, the control input parameter is the duty ratio $d$, and the control output parameter is the output voltage $V_O$, with other parameters being disregarded.

Because the system transfer function has a zero on the right side of the s-plane, the root locus method is going to be used to design the system control. From the root locus plot, which is developed by MATLAB, the control gain $K$ with the best step response is chosen for the control design.

The algorithm used in this project is the Perturb and Observe (P&O) approach. Its operational principle relies on continuously comparing the input voltage and power. Based on the comparison results, a decision is made to either increase or decrease the PV array's voltage to optimize performance. This increase or increase in the PV voltage has to be limited through a saturation block with the PV array's maximum and minimum voltages of 90 V and 80 V, respectively.

After designing the control of the system by tuning its parameters and determining the appropriate control gain, the system is able to track the maximum power. It shows a good response by tracking MPP at the presence of disturbance, such as

a drop in the insulation or alteration to the load value.

## List of abbreviations

| | |
|---|---|
| A | Ampere |
| BJT | Bipolar junction transistor |
| CCM | Continuous conduction mode |
| CV | Constant voltage |
| DC–DC | Direct current to direct current |
| FLC | Fuzzy logic control |
| GMPP | Global maximum power point |
| IC | Incremental conductance |
| IGBT | Insulated gate bipolar transistor |
| IWO | Invasive weed optimization |
| KW | Kilowatt |
| MPP | Maximum power point |
| MPPT | Maximum power point tracker |
| ms | Millisecond |
| P&O | Perturb and observe |
| PI | Proportional integral |
| PSO | Particle swarm optimization |
| PV | Photovoltaic |
| SCC | Short circuit current |
| SISO | Single-input single-output |
| STC | Standard test conditions |
| V | Volt |

## Compliance with ethical standards

## Conflict of interest

The author(s) declared no potential conflicts of interest with respect to the research, authorship, and/or publication of this article.

## References


Abbas A, Farhan M, Shahzad M, Liaqat R, and Ijaz U (2025). Power tracking and performance analysis of hybrid perturb–observe, particle swarm optimization, and fuzzy logic-based improved MPPT control for standalone PV system. Technologies, 13(3): 112. https://doi.org/10.3390/technologies13030112

Al-Baidhani H, Corti F, Reatti A, and Kazimierczuk MK (2023). Robust sliding-mode control design of DC-DC zeta converter operating in buck and boost modes. Mathematics, 11(17): 3791. https://doi.org/10.3390/math11173791

Ali Z, Abbas SZ, Mahmood A, Ali SW, Javed SB, and Su CL (2023). A study of a generalized photovoltaic system with MPPT using perturb and observer algorithms under varying conditions. Energies, 16(9): 3638. https://doi.org/10.3390/en16093638

Anbuchandran S, Stephen DS, Babu MA, and Bhuvanesh A (2024). MIWO based MPPT of PV system for induction motor driven water pumping system. E-Prime – Advances in Electrical Engineering, Electronics and Energy, 10: 100835. https://doi.org/10.1016/j.prime.2024.100835

Anowar MH and Roy P (2019). A modified incremental conductance based photovoltaic MPPT charge controller. In the International Conference on Electrical, Computer and Communication Engineering (ECCE), IEEE, Cox's Bazar, Bangladesh: 1-5. https://doi.org/10.1109/ECACE.2019.8679308

Byanpambé G, Djondiné P, Guidkaya G et al. (2024). A modified fractional short circuit current MPPT and multicellular converter for improving power quality and efficiency in PV chain. PLOS ONE, 19(9): e0309460. https://doi.org/10.1371/journal.pone.0309460 **PMid:39226281 PMCid:PMC11371253**

Celikel R, Yilmaz M, and Gundogdu A (2022). A voltage scanning-based MPPT method for PV power systems under complex partial shading conditions. Renewable Energy, 184: 361-373. https://doi.org/10.1016/j.renene.2021.11.098

Cubas J, Pindado S, and Sorribes-Palmer F (2017). Analytical calculation of photovoltaic systems maximum power point (MPP) based on the operation point. Applied Sciences, 7(9): 870. https://doi.org/10.3390/app7090870

Deraz SA, Zaky MS, Tawfiq KB, and Mansour AS (2024). State space average modeling, small signal analysis, and control implementation of an efficient single-switch high-gain multicell boost DC-DC converter with low voltage stress. Electronics, 13(16): 3264. https://doi.org/10.3390/electronics13163264

Endiz MS, Gökkuş G, Coşgun AE, and Demir H (2025). A review of traditional and advanced MPPT approaches for PV systems under uniformly insolation and partially shaded conditions. Applied Sciences, 15(3): 1031. https://doi.org/10.3390/app15031031

Ganesan P and Gunasekaran S (2022). Modelling and simulation of incremental conductance algorithm for solar maximum power point tracker. In the IEEE Delhi Section Conference, IEEE, New Delhi, India: 1-6. https://doi.org/10.1109/DELCON54057.2022.9753007

Garcia AS and Strandberg R (2021). Analytical modeling of the maximum power point with series resistance. Applied Sciences, 11(22): 10952. https://doi.org/10.3390/app112210952

Gil-Velasco A and Aguilar-Castillo C (2021). A modification of the perturb and observe method to improve the energy harvesting of PV systems under partial shading conditions. Energies, 14(9): 2521. https://doi.org/10.3390/en14092521

Guerra MI, Ugulino de Araújo FM, Dhimish M, and Vieira RG (2021). Assessing maximum power point tracking intelligent techniques on a PV system with a buck–boost converter. Energies, 14(22): 7453. https://doi.org/10.3390/en14227453

Gul S, Malik SM, Sun Y, and Alsaif F (2024). An artificial neural network based MPPT control of modified flyback converter for PV systems in active buildings. Energy Reports, 12: 2865-2872. https://doi.org/10.1016/j.egyr.2024.08.082

Hamad SA, Ghalib MA, Munshi A, Alotaibi M, and Ebied MA (2025). Evaluating machine learning models comprehensively for predicting maximum power from photovoltaic systems. Scientific Reports, 15: 10750. https://doi.org/10.1038/s41598-025-91044-6 **PMid:40155411 PMCid:PMC11953328**

Hamidi F, Olteanu SC, Popescu D, Jerbi H, Dincă I, Ben Aoun S, and Abbassi R (2020). Model based optimisation algorithm for maximum power point tracking in photovoltaic panels. Energies, 13(18): 4798. https://doi.org/10.3390/en13184798

Hinov N, Gocheva P, and Gochev V (2023). Index matrix-based modeling and simulation of buck converter. Mathematics, 11(23): 4756. https://doi.org/10.3390/math11234756

Ibrahim MH, Ang SP, Dani MN, Rahman MI, Petra R, and Sulthan SM (2023). Optimizing step-size of perturb and observe and incremental conductance MPPT techniques using PSO for grid-tied PV system. IEEE Access, 11: 13079-13090. https://doi.org/10.1109/ACCESS.2023.3242979

Khan MU, Murtaza AF, Noman AM, Sher HA, and Zafar M (2024). State-space modeling, design, and analysis of the DC-DC converters for PV application: A review. Sustainability, 16(1): 202. https://doi.org/10.3390/su16010202

Koundi M, El Idrissi Z, El Fadil H et al. (2022). State-feedback control of interleaved buck–boost dc–dc power converter with continuous input current for fuel cell energy sources: Theoretical design and experimental validation. World

Electric Vehicle Journal, 13(7): 124. https://doi.org/10.3390/wevj13070124

Mahmod Mohammad AN, Mohd Radzi MA, Azis N, Shafie S, and Atiqi Mohd Zainuri MA (2020). An enhanced adaptive perturb and observe technique for efficient maximum power point tracking under partial shading conditions. Applied Sciences, 10(11): 3912. https://doi.org/10.3390/app10113912

Maidin SN, Kamardin K, Ahmad NA, Ahmed IS, Kaidi HM, Bani NA, and Ambran S (2020). Algorithms and methods for energy harvesting in wireless networks: A review. International Journal of Advanced and Applied Sciences, 7(1): 125–138. https://doi.org/10.21833/ijaas.2020.01.013

Masry MZE, Mohammed A, Amer F, and Mubarak R (2023). New hybrid MPPT technique including artificial intelligence and traditional techniques for extracting the global maximum power from partially shaded PV systems. Sustainability, 15(14): 10884. https://doi.org/10.3390/su151410884

Melhaoui M, Rhiat M, Oukili M et al. (2025). Hybrid fuzzy logic approach for enhanced MPPT control in PV systems. Scientific Reports, 15: 19235. https://doi.org/10.1038/s41598-025-03154-w **PMid:40456858 PMCid:PMC12130274**

Obeidi N, Kermadi M, Belmadani B, Allag A, Achour L, and Mekhilef S (2022). A current sensorless control of buck-boost converter for maximum power point tracking in photovoltaic applications. Energies, 15(20): 7811. https://doi.org/10.3390/en15207811

Restrepo C, Yanēz-Monsalvez N, González-Castaño C, Kouro S, and Rodriguez J (2021). A fast converging hybrid MPPT algorithm based on abc and P&O techniques for a partially shaded PV system. Mathematics, 9(18): 2228. https://doi.org/10.3390/math9182228

Ríos J, Enrique JM, Barragán AJ, and Andújar JM (2020). Comparative analysis of robustness and tracking efficiency of maximum power point in photovoltaic generators, using estimation of the maximum power point resistance by irradiance measurement processing. Sensors, 20(24): 7247. https://doi.org/10.3390/s20247247 **PMid:33348793 PMCid:PMC7766423**

Salman S, Ai X, and Wu Z (2018). Design of a P-and-O algorithm based MPPT charge controller for a stand-alone 200W PV system. Protection and Control of Modern Power Systems, 3: 25. https://doi.org/10.1186/s41601-018-0099-8

Shang L, Guo H, and Zhu W (2020). An improved MPPT control strategy based on incremental conductance algorithm. Protection and Control of Modern Power Systems, 5(2): 1-8. https://doi.org/10.1186/s41601-020-00161-z

Tirado-Serrato JG, Garcia AS, and Maximov S (2024). Analytical computation of the maximum power point of solar cells using perturbation theory. Energies, 17(23): 6035. https://doi.org/10.3390/en17236035

Tomaszuk A and Borawski K (2024). A new approach to examine the dynamics of switched-mode step-up DC–DC converters: A switched state-space model. Energies, 17(17): 4413. https://doi.org/10.3390/en17174413

Xie L, Wan D, and Qin R (2023). Dual-loop voltage–current control of a fractional-order buck-boost converter using a fractional-order $PI^{\lambda}$ controller. Fractal and Fractional, 7(3): 256. https://doi.org/10.3390/fractalfract7030256

Yilmaz M (2024). Comparative analysis of hybrid maximum power point tracking algorithms using voltage scanning and perturb and observe methods for photovoltaic systems under partial shading conditions. Sustainability, 16(10): 4199. https://doi.org/10.3390/su16104199

Zambrano-Gutierrez DF, Cruz-Duarte JM, Valencia-Rivera GH, Amaya I, and Avina-Cervantes JG (2022). Dynamic analysis for the physically correct model of a fractional-order buck-boost converter. Computer Sciences and Mathematics Forum, 4(1): 2. https://doi.org/10.3390/cmsf2022004002